# The Intimin periplasmic domain mediates dimerisation and binding to peptidoglycan

Jack C. Leo[1,5], Philipp Oberhettinger[2], Manish Chaubey[1], Monika Schütz[2], Daniel Kühner[3], Ute Bertsche[3], Heinz Schwarz[1], Friedrich Götz[3], Ingo B. Autenrieth[2], Murray Coles[1], Dirk Linke[1,4*]

[1]Max Planck Institute for Developmental Biology, Department of Protein Evolution, 72076 Tübingen, Germany

[2]Interfaculty Institute for Microbiology and Infection Medicine, University Clinics Tübingen, 72076 Tübingen, Germany

[3]Department of Microbial Genetics, University of Tübingen, 72076 Tübingen, Germany

[4]Department of Biosciences, University of Oslo, 0316 Oslo, Norway

[5]Current address: Department of Biosciences, University of Oslo, 0316 Oslo, Norway

[*]Corresponding author. E-mail: dirk.linke@ibv.uio.no

**Running title:** Functions of the Intimin periplasmic domain

**Keywords**: Intimin/Invasin/inverse autotransporter/lysin motif/peptidoglycan

**SUMMARY**

Intimin and Invasin are prototypical inverse (Type Ve) autotransporters and important virulence factors of enteropathogenic *Escherichia coli* and *Yersinia spp*., respectively. In addition to a C-terminal extracellular domain and a β-barrel transmembrane domain, both proteins also contain a short N-terminal periplasmic domain that, in Intimin, includes a lysin motif (LysM), which is thought to mediate binding to peptidoglycan. We show that the periplasmic domain of Intimin – but not the shorter domain of Invasin – does bind to peptidoglycan both *in vitro* and *in vivo*, but only under acidic conditions. We present the solution structure of the Intimin LysM, which has an additional, potentially functionally relevant α-helix compared to other LysMs. In contrast to previous reports, we demonstrate that the periplasmic domain of Intimin mediates dimerisation. Our data suggests that the periplasmic domain contains two dimerisation interfaces. We further show that dimerisation and peptidoglycan binding are general features of LysM-containing inverse autotransporters. The periplasmic domain could be involved in autotransport, and peptidoglycan binding may aid in resisting mechanical and chemical stress during transit through the gastrointestinal tract.

## INTRODUCTION

An often essential first step in host colonization by bacterial pathogens is the adherence of bacteria to host cells and tissues. This binding is mediated by various adhesins, many of which are proteinaceous molecules expressed on the cell surface. Intimin (Int) is a major adhesin of enteropathogenic and enterohaemorrhagic *Escherichia coli* (EPEC and EHEC) and is instrumental in the formation of actin pedestals leading to attaching and effacing (A/E) lesions on enterocytes (Schmidt, 2010). It is a homologue of Invasin (Inv) from enteropathogenic *Yersinia spp*., which mediates direct binding to host cells *via* $\beta_1$ integrins (Leo and Skurnik, 2011). However, unlike Inv, Int does not bind primarily to a cellular receptor; rather, the Int receptor Tir is produced by the bacteria themselves and transferred to the host cell membrane through the type 3 secretion system (Schmidt, 2010).

The extracellular domain of Intimin consists of tandem immunoglobulin (Ig)-like domains capped by a C-type lectin domain (Kelly *et al.*, 1999). The Tir-binding region is located in the C-terminal superdomain consisting of the last Ig domain and the lectin domain (Luo *et al.*, 2000). The extracellular portion of Invasin has a similar structure (Hamburger *et al.*, 1999), and the integrin-binding region is also located at the C-terminal tip of the protein (Leong *et al.*, 1990). The extracellular or passenger domain of both proteins is exported by a type Ve or inverse autotransport mechanism: a 12-stranded transmembrane β-barrel N-terminal to the passenger domain acts as a translocation pore which facilitates the secretion of the passenger domain across the outer membrane (Oberhettinger *et al.*, 2012; Leo *et al.*, 2012; Fairman *et al.*, 2012).

In addition to the passenger and translocation domains, both proteins contain a small N-terminal periplasmic domain, also referred to as the α-domain (Tsai *et al.*, 2010). In Int, the periplasmic domain contains a lysin motif (LysM) found in many peptidoglycan-binding proteins (Buist *et al.*, 2008). The LysM is a small domain consisting of a 2-stranded anti-parallel β-sheet packed against two α-helices with the topology β-α-α-β (Bateman and Bycroft, 2000). LysMs usually bind to the N-acetylglucosamine moieties in peptidoglycan (PGN) and chitin, or other carbohydrate structures (Buist *et al.*, 2008). In contrast to Int, the Inv periplasmic region lacks a LysM.

Due to the presence of a LysM in the Int periplasmic domain, it has long been suspected that the periplasmic domain would mediate binding to PGN (*e.g*. Bateman and Bycroft, 2000; Tsai *et al.*, 2010; Pisano *et al.*, 2012). However, up to now, this hypothesis has not been experimentally validated. In this study, we show that the periplasmic domain of Int does indeed bind PGN, but only under acidic

conditions. In addition, we show that the periplasmic domain mediates dimerisation of Int. In contrast, the shorter periplasmic domain of Inv has neither of these functions. We also present a solution structure of the Int LysM and show that dimerisation and PGN binding are conserved functions of LysMs of inverse autotransporters. Dimerisation appears to be an important feature for the virulence function of these proteins. Our results show that the periplasmic domain of type Ve autotransporters are functional and may be involved in stabilising the cell envelope and virulence functions.

## RESULTS

### *Bioinformatic analysis of periplasmic domains from inverse autotransporters*

Secondary structure prediction of the Int sequence using software of the online Bioinformatics Toolkit of the Max-Planck Institute for Developmental Biology (http://toolkit.tuebingen.mpg.de/) reveals that the periplasmic domain contains the LysM motif, consisting of a small β-sheet packed against two α-helices, followed C-terminally by two closely spaced α-helices (Fig. 1A). There is an unstructured loop of approximately 30 residues linking the LysM domain to the first of the C-terminal helices, which we call the spacer sequence. The periplasmic domain of Inv also contains the helices, but lacks the LysM motif (Fig. 1A). An alignment of selected members of the Inv-Int family periplasmic domains shows that the C-terminal helices are conserved, whereas the LysM motif is only present in some members of the family (Fig. S1). Similar results were also obtained in an earlier study (Tsai *et al.*, 2010).

To investigate the distribution of different types of periplasmic domains within inverse autotransporters, we performed clustering analysis of the periplasmic domain sequences using CLANS (Frickey and Lupas, 2004). A total of 172 sequences were included in the clustering (Table S1), and after singletons (sequences with *P*-values for BLAST high-scoring segment pairs higher than 0.99) were removed 152 sequences remained. The results (Fig. 1B) show that the periplasmic domains cluster largely based on taxonomic distribution rather than length or the presence of the LysM motif. Most of the sequences were derived from the γ-Proteobacteria, especially the Enterobacteriaceae, which form a large cluster. Int is located close to the centre of this cluster, whereas Inv is located more peripherally (Fig. 1B). Other distinct clusters are formed by cyanobacterial sequences and sequences from the β-proteobacterial genus *Bordetella*. Interestingly, periplasmic domains from the cyanobacterial genus *Synechococcus* form two distinct clusters that are only distantly connected to the enterobacterial cluster; however, as the synechococcal sequences are all very short, the separate clusters may be artefactual. The sizes of the sequences do not have a large effect on the clustering, as both large and small sequences are found in

the same clusters (Fig. S2A). The LysM appears restricted to the large γ-proteobacterial cluster, as it was not detected in any of the other groups (Fig. 1C). The presence of the LysM domain can to some degree be predicted based on the length of the protein sequence; however, the correlation is not absolute and there are several large members of the family lacking the LysM motif (Fig. S2B). The prevalence of LysMs in large inverse autotransporters suggests that the LysM may be involved in the autotransport process, possibly stabilising translocation intermediates during secretion.

***The Int periplasmic domain mediates dimerisation***

Int has been reported to form dimers *via* its β-barrel domain (Touzé *et al.*, 2004). However, the Int β-barrel crystallises as a monomer (Fairman *et al.*, 2012). This suggested to us that the dimerisation might be mediated by the periplasmic domain, which was included in the construct used by Touzé *et al* (2004). To test this, we produced the periplasmic domains of Int (from EPEC) and Inv (from *Y. enterocolitica*) as maltose-binding protein (MBP) fusions, named IntPeri-MBP and InvPeri-MBP, with the MBP as a C-terminal fusion and a hexahistidine tag on the N-termini of the periplasmic domains. The constructs are depicted schematically in Fig. 2A, and all plasmids used in the study are summarised in Table 1. IntPeri-MBP in particular is unstable, and degradation products were observed in cell lysates (data not shown); however, we were able to purify the proteins to high purity by passing the proteins through both a nickel and amylose column followed by size exclusion chromatography (SEC).

When we performed analytical SEC at physiological pH (7.4.), MBP and InvPeri-MBP run at the expected sizes of the monomer, whereas IntPeri-MBP gives two peaks: the major peak migrates at an apparent size slightly larger than the dimer and the smaller peak at the expected molecular weight of the monomer (Fig. 2B). Both peaks contain Int-MBP, suggesting an equilibrium between monomeric and dimeric forms. Indeed, when we reran the major peak through the SEC column, a similar distribution for dimer and monomer was observed (Fig. S3A).

To further characterise the region in the periplasmic domain responsible for dimerisation, we fused short fragments of the Int periplasmic domain to MBP (Fig. 2A). These fragments were the LysM domain along with the spacer sequence (IntLysM-MBP), the two C-terminal helices (IntPeriHelix1-MBP) or just the second, C-terminal helix (IntPeriHelix2-MBP). In SEC, IntLysM-MBP migrates as a dimer, whereas the other two constructs run as a monomer (Fig. 2C). This suggests that the N-terminal region of the periplasmic domain is the dimerisation interface.

Touzé and coworkers showed that the β-barrel and flanking regions (residues 189-550) contains a dimerisation site (Touzé *et al.*, 2004). As the β-barrel itself is monomeric, Fairman *et al*. speculated that the dimerisation interface would either be in the periplasmic region or the first extracellular Ig-like domain (D00) (Fairman *et al.*, 2012). Our results above suggest a dimerisation site in or near the LysM. We therefore produced and purified the D00 domain and tested its oligomerisation status by SEC. The domain ran as a monomer (Fig. S4). Thus, the dimerisation observed by Touzé *et al* must be due to the short stretch preceding the β-barrel domain (residues 189-209). This corresponds to C-terminal helix in the periplasmic domain (Helix2). This helix failed to dimerise when fused to MBP, but it is possible that the helix is not correctly folded outside its native context. We therefore submit that the Int periplasmic domain contains two dimerisation interfaces, the LysM region and Helix2, though the latter only mediates dimer formation when fused to the β-barrel.

***The periplasmic domains of Int and Inv promote surface display of the passenger domain***

To investigate the relevance of the periplasmic domain under *in vivo* conditions, we produced deletion mutants of Inv and Int in *E. coli.* We used full-length, wild-type (wt) Int and a construct missing the entire periplasmic domain (IntΔPeri). We did the same for Inv (Inv wt and InvΔPeri), and bacteria with the empty vector (pASK-IBA2) acted as our negative control. In addition, we made two chimaeric constructs: IntPeri-Inv, where the periplasmic domain of Inv was switched to that of Int, and InvPeri-Int, where the Int periplasmic domain was replaced with the Inv periplasmic domain. These constructs are summarized schematically in Fig. 3A.

To determine whether the truncations had a major effect on Int biogenesis, we examined the surface display of the Int passenger by both fluorescence-activated cell sorting (FACS) and immunofluorescence microscopy. Both Int wt and Inv wt were exported to the surface (Fig. 3B). The ΔPeri constructs were also surface-exposed but displayed a bimodal distribution, with a part of the population exhibiting lower fluorescence. This may be due to impaired secretion of the passenger domain. In contrast, the chimaeras were more fluorescent than the corresponding wt constructs, suggesting higher expression levels or more efficient surface display. The reason for this is unclear.

We also examined the effect of the truncations and domain switching on adhesion and induction of interleukin (IL)-8. For Int, we performed qualitative adhesion assays, where we examined the adherence of the omp2 strain containing the Int constructs to HeLa cells that had been preinfected with a *ΔeaeA* EPEC strain to prime the cells with Tir (Oberhettinger *et al.*, 2012). The wild-type construct adhered

strongly to preinfected cells, but not to uninfected cells (Fig. 3C). However, IntΔPeri showed much lower adhesion than the wt, probably because of reduced surface display, but possibly also because of reduced avidity through the loss of dimer formation (Fig. 3C). The chimaeric construct InvPeri-Int promoted intermediate adhesion; stronger than IntΔPeri, but not as strong as the wt, despite high surface exposure. We assume this is due to the lack of dimer formation and thus a loss of co-operativity in the Int-Tir interaction (Touzé *et al.*, 2004). The empty vector served as a background control.

For the Inv constructs, we measured the induction of IL-8 production in infected cells with an enzyme-linked immunosorbent assay (ELISA). Wild-type Inv induced IL-8 well over background levels, as did the positive control tumor necrosis factor (TNF) (Fig. 3D). The vector control was barely above background levels, and IL-8 production by InvΔPeri was reduced compared to the wt. However, IntPeri-Inv showed significantly higher induction of IL-8 than even TNF. This increase is presumably largely due to the Int periplasmic domain mediating dimerisation of Inv, but the higher levels of IntPeri-Inv on the surface may also have an effect (Fig. 3B). In *Y. pseudotuberculosis*, Inv contains an additional extracellular domain (D2) that mediates self-association and leads to more efficient bacterial uptake than in *Y. enterocolitica* (Dersch and Isberg, 1999; Dersch and Isberg, 2000). In the chimaeric IntPeri-Inv, the Int periplasmic domain could thus fulfil a role similar to D2, leading to dimerisation which in turn promotes receptor clustering, more efficient cell invasion and higher IL-8 levels.

***The periplasmic domain of Int, but not Inv, binds peptidoglycan in a pH-dependent manner***

We performed pull-down assays with our MBP fusions using purified PGN sacculi from *E. coli* to determine whether the Int periplasmic domain binds PGN (Fig. 4). We fortuitously found that binding was strongest at low pH: in assays performed at pH 5.0, approximately half the IntPeri-MBP fusion precipitates with the sacculi, while the MBP control remain in the supernatant (Fig. 4A). In this assay, Inv-MBP displayed only background-level binding to PGN (Fig. 4A). In the absence of PGN, all three proteins remained soluble. At normal physiological pH (7.4), however, we saw no binding of IntPeri-MBP to PGN, with most of the protein remaining in the supernatant (Fig. 4A).

To examine the effect of pH on the binding of IntPeri-MBP to PGN more systematically, we performed binding at range of pH values between 8.0 and 3.0; strong binding first became evident at pH 6.0 and the ratio of bound IntPeri-MBP to soluble protein remains constant even with reduction in pH value (Fig. 4B). In the control experiment without PGN sacculi, the protein remains soluble at all pH values tested (Fig. 4B). We observed similar results with a glutathione-S-transferase (GST) fusion of IntPeri; however,

GST itself tends to precipitate at low pH, which made interpreting these results difficult (data not shown). Int-MBP still dimerises at pH 4.0 (Fig. S3B), demonstrating that dimerisation is independent of pH.

Physiologically abundant divalent cations ($Ca^{2+}$, $Mg^{2+}$, $Mn^{2+}$, $Zn^{2+}$) might have an effect on the binding of IntPeri to PGN. To check this, we added these ions as chloride salts to the pull-down assay, and in addition we tested the effect of the chelators ethylene diamine tetra-acetic acid (EDTA) and sodium citrate. However, neither the divalent cations nor the chelators had an effect on binding, though some of the ions, particularly $Ca^{2+}$, slightly modified the pattern of migration in SDS-PAGE (Fig. 4C). We therefore conclude that the binding of IntPeri to peptidoglycan is pH-dependent but does not require divalent ions.

We partially digested peptidoglycan sacculi with mutanolysin and performed a competition assay with the soluble digestion products. Addition of the degradation products inhibited the binding of IntPeri-MBP to the sacculi in a dose-dependent manner, though we did not observe complete inhibition of binding to sacculi (Fig. 4D). This demonstrates that soluble muropeptides can compete for binding to IntPeri-MBP. Many LysM-containing proteins also bind chitin (Buist *et al.*, 2008). We therefore ran IntPeri-MBP, InvPeri-MBP and MBP as a control through a chitin column. However, we did not observe binding for any of the constructs (Fig. 4E). This suggests that IntLysM binds to other determinants in PGN than the N-acetylglucosamine – N-acetylmuramic acid backbone.

To find out which part of the periplasmic domain of Int is responsible for PGN binding, we performed pull-down assays with IntLysM-MBP, IntPeriHelix1-MBP and IntPeriHelix2-MBP (Fig. 4F). In this assay, only IntLysM-MBP coprecipitated with the sacculi in appreciable amounts, demonstrating that it is indeed the LysM that mediates PGN binding.

As we saw some background levels of InvPeri-MBP bound to PGN, we wished to further investigate the relative affinities of InvPeri-MBP and IntPeri-MBP. To this end, we performed pull-down assays using a concentration series of IntPeri-MBP and InvPeri-MBP with a constant amount of PGN. At low concentrations of IntPeri-MBP, almost all the protein is pulled down with the sacculi, whereas the fraction in the pellet decreases steadily with increasing protein concentration (Fig. 5A). InvPeri-MBP follows a similar trend, but even at low concentrations only approximately 50% is pulled down with the sacculi, and at higher concentrations less than 20% remains in the pellet (Fig. 5A). In the reverse experiment, where we varied the concentration of PGN but kept the protein concentration constant,

only a small fraction of IntPeri-MBP precipitates with low amounts of PGN, but as the amount of PGN rises, increasingly more IntPeri-MBP is found in the pellet (Fig. 5B). The increase in roughly linear, and at the highest concentration tested (50 µg), 75% of the protein is in the pellet. Again, InvPeri-MBP follows a similar trend, but the increase in the fraction of pelleted protein is not as large, and at most only 30% of the protein was pulled down with the sacculi (Fig. 5B). It appears that IntPeri-MBP binds with high affinity to PGN, as most of the protein precipitates at low protein concentration. However, the fraction of bound protein declines more or less linearly with increasing concentration of IntPeri-MBP, which we interpret to mean that there are a limited number of high-affinity binding sites in the sacculi and that these are quickly saturated. The amount of IntPeri-MBP scales linearly with increasing PGN, which is consistent with this interpretation. However, also InvPeri-MBP follows similar trends, though the binding levels are much lower than for IntPeri-MBP. When we incubated sacculi with both IntPeri-MBP and InvPeri-MBP, we did not see any effect of high concentrations of InvPeri-MBP on the binding levels of IntPeri-MBP, suggesting that these proteins do not compete for the same binding site(s) and that the binding of InvPeri-MBP is indeed unspecific (Fig. S5). The results obtained using concentration series of either protein or PGN should be viewed with caution, however, as the assays used are rather crude and include washing steps which we did not take into account when calculating the relative binding, and even in the absence of PGN we often observe faint background bands in the pellets (Fig. 4). In addition, the pull-down assays do not cover a wide enough range to estimate reliable dissociation constants. Our tentative conclusions are therefore that IntPeri-MBP binds with high affinity to a finite number of binding sites, whereas a small amount of InvPeri-MBP precipitates unspecifically with the sacculi, though we cannot rule out some specific but low-affinity interaction. Unfortunately, we could not use more sophisticated biophysical methods such as surface plasmon resonance to more accurately estimate the dissociation constants due to the difficulty of immobilising sacculi on detector chips.

### ***The Int periplasmic domain binds to PGN* in vivo**

To determine whether the Int periplasmic domain can mediate PGN binding *in vivo*, we cloned the MBP fusions into pIBA2C, which contains a signal sequence for periplasmic targeting. We used chloramphenicol selection rather than ampicillin in order to avoid any structural changes to PGN. The protein was expressed in medium buffered at either pH 7.4 or pH 5.5. To see if the MBP fusion proteins bound to PGN, we extracted the periplasmic fraction by osmotic shock. All solutions were buffered at either pH 7.4 or pH 5.5. We then detected the protein by Western blot using an anti-MBP antiserum. For the whole-cell samples of IntPeri-MBP, a strong band is evident at ~65 kDa, as expected, along with a

small amount of apparent degradation products (Fig. 6A). We assume the 65 kDa band corresponds to intact IntPeri-MBP. At pH 7.4, this band is also in the periplasmic fraction, but at pH 5.5 the 65 kDa band is barely visible. InvPeri-MBP is less stable, with two stronger bands: ~50 kDa, which is presumably the intact protein, and ~45 kDa, which we assume is a degradation product. Both bands are present at similar levels in all samples. The vector control does not display any bands, demonstrating the specificity of the antiserum, whereas in our control for periplasmic extraction (pIBA2C-MBP), the MBP band (41 kDa) is present in all the samples at an equal intensity. As the 65 kDa IntPeri-MBP band is present in the periplasmic fraction at pH 7.4 but not at pH 5.5, we interpret this to mean that at pH 5.5, IntPeri-MBP is retained in the periplasm due to PGN binding. This finding is consistent with our pull-down assays, as is the observation that InvPeri-MBP is extracted at similar amounts at both pH values, which supports the conclusion that it does not bind to PGN.

***Structure of the Intimin LysM***

To date, there is no structural information about the inverse autotransporter periplasmic domains. To structurally characterise the periplasmic domain, we produced and purified the N-terminal region of the Int periplasmic domain (residues 40-153). We did this by producing the protein as a fusion with MBP, followed by cleaving the MBP from the Int fragment with tomato etch virus (TEV) protease. This region contains the predicted LysM domain (residues 63-114) and putative dimerisation interface (Fig. 2C). We then proceeded to solve the solution structure of this region using nuclear magnetic resonance (NMR) spectroscopy.

When measuring the NMR spectra, we noted the rapid decay of several signals with shifts suggesting a structured environment and the appearance of others more consistent with unstructured protein chain. The signals appearing were assigned to the C-terminus of the protein, *i.e.* in the spacer sequence. Despite extensive efforts, we could not obtain high-resolution structural information from the transient signals, although chemical shifts suggest that this region has considerable β-sheet content. We conclude that this structure is unstable and unfolds once the C-terminal fusion partner is removed. At equilibrium, both the N-terminus (residues 40-60) and the C-terminus (residues 115-143) are disordered (Fig. 7A). However, the LysM itself was well defined (Fig. 7A). The NMR constraint and refinement statistics are presented in Table S2. It is noteworthy that we could not detect the dimerisation interface in NMR measurements on mixtures of differentially labelled protein. This is probably due to the unfolding of the spacer sequence that presumably contains the dimerisation site.

The overall fold of the Int LysM is the typical β-α-α-β seen in other LysM structures (Fig. 7B). A Cα superposition of the various LysMs shows that the main chain conformation is largely similar (Fig. 7C), with the root mean square deviation (RMSD) between the different structures and the Int LysM varying from 1.28 Å to 3.62 Å. Most of the LysM structures have an RMSD between 1.5 and 2.5 Å; the furthest outliers are the hypothetical human protein SB145 (Protein database ID 2DJP) at 2.75 Å and the gpX LysM from coliphage P2 (2LTF; (Maxwell *et al.*, 2013)) with an RMSD of 3.62 Å. The closest structure is from the putative (trans)peptidase YkuD from *Bacillus subtilis* (Bielnicki *et al.*, 2006). Though there are no major differences between the current LysM domain structures, the Int LysM does contain a short α-helix connecting the structurally conserved C-terminal α-helix and the C-terminal β-strand (Fig. 7C). Though gpX some other LysMs have a helical turn in this region, these are not as long and defined as the α-helix in the Int LysM. This extra helix was predicted by bioinformatics (Fig. S1), and appears conserved within the inverse autotransporter LysMs, suggesting it has some function. Future work will be needed to uncover the relevance of this α-helix.

***PGN binding and dimerisation are general features of LysM-containing inverse autotransporters***

Several inverse autotransporters from the Enterobacteriaceae contain a periplasmic LysM domain (Fig. 1). To test whether binding to PGN and dimerisation are general features of inverse autotransporter LysMs, we cloned the LysM-containing periplasmic domain from an Inv homologue from the fish pathogen *Yersinia ruckeri* (GI: 238705545), which we refer to as YrInv for *Y. ruckeri* Invasin. We produced the periplasmic domain as an MBP fusion (YrInvPeri-MBP). During later purification steps, we noticed that in SDS-PAGE, the band of the expected size (58 kDa) began to lose intensity and a new band migrating at ~200 kDa appeared, and almost all the protein was in this higher molecular-weight band after the SEC step. This suggested to us that YrInv was forming multimers stabilised by disulphide bridges, which were not disrupted in our SDS-PAGE experiments because we do not routinely add reducing agent to our sample buffer. When we used reducing sample buffer, all the protein previously in the ~200 kDa band ran at the expected size of the monomer, showing that the multimer resulted from the formation of disulphides by oxidation during purification (Figure 8A). Indeed, there is a single cysteine in the periplasmic domain in the spacer sequence between the LysM and Helix1 which presumably mediates the disulphide formation (Fig. 8D). When we performed analytical SEC, YrInvPeri-MBP migrated with an apparent size of ~240 kDa (Fig. 8B). However, if the buffer was supplemented with dithiothreitol (DTT), the protein migrated with an apparent molecular weight of 91 kDa (Fig. 8B). As the expected size of the monomer is 58 kDa, we interpret the 91 kDa peak to represent the dimeric form

of the molecule. The 240 kDa peak seen under non-reducing conditions would therefore correspond to a tetrameric molecule, *i.e.* a dimer of dimers stabilised by disulphides. We are not sure whether this tetramer represents the physiological quaternary structure of YrInv, as we were unable to express the full-length protein in *E. coli*. Though this tetramer could be an artefact of the purification procedure, it seems more likely that the tetrameric form is the physiologically relevant one, as the tetramer of YrInvPeri-MBP forms quantitatively in the presence of oxygen, and disulphides would be formed in the periplasm. Interestingly, in addition to dimerising, Inv from *Y. pseudotuberculosis* also forms tetramers (Dersch and Isberg, 1999), further pointing towards the interpretation of the tetramer being the physiologically relevant form of YrInv.

We also performed pull-down assays with PGN sacculi. In the pull-down assay, approximately half the protein precipitated with the sacculi at pH 5.0, similar to Int, whereas in the control reaction the protein remained soluble (Fig. 8C). Addition of DTT did not have a significant effect on the amount of protein in the pellet fraction, suggesting that the tetrameric form is not required for PGN binding (Fig. 8C). Interestingly, similar to Int, YrInvPeri-MBP did not bind to PGN at pH 7.4 (Fig. 8C). These results show that also YrInv-MBP dimerises, and probably further tetramerises, and binds to PGN. This suggests that dimerisation and PGN binding are general properties of LysM-containing periplasmic domains of inverse autotransporters, and that the pH dependence of the PGN interaction may also be a general feature.

## DISCUSSION

### *PGN binding by the Intimin LysM*

Here, we provide the first experimental evidence to show that the Int periplasmic region has affinity for PGN. In addition, we present the NMR structure of the Int LysM, giving the first structural information on an inverse autotransporter periplasmic domain. Using pull-down assays with purified PGN sacculi, we were able to experimentally show, for the first time, that the LysM of the Int periplasmic domain mediates binding to PGN, whereas the periplasmic domain from Inv did not bind with appreciable affinity. In our *in vivo* experiments, InvPeri-MBP was efficiently extracted from the periplasm at pH 5.5., whereas IntPeri-MBP was retained. These data all point to IntPeri binding strongly to PGN, whereas InvPeri binds only at low levels, which we contend represent unspecific background binding. An arguable shortcoming of our experiments is that were not able to test the binding of InvPeri to PGN from *Y. enterocolitica*. However, the composition of PGN from *E. coli* and *Y. enterocolitica* is very similar, though there is some variation in the relative abundance of specific muropeptides (Quintela *et al.*, 1995). This

suggests that if Inv did bind with high affinity to PGN, we would see stronger binding in our experiments. This view is supported by the fact that YrInvPeri clearly does bind to PGN from *E. coli* (Fig. 7). Our conclusion is therefore that only LysM-containing inverse autotransporter periplasmic domains mediate PGN binding.

Most LysM-containing proteins that have been studied bind to the carbohydrate backbone of PGN, and many also bind to the N-acetylglucosamine backbone of chitin. However, we did not detect any binding to chitin beads. Furthermore, although we observed strong binding by IntPeri-MBP to purified sacculi, the binding saturates at a rather low concentration of protein in relation to PGN (Fig. 5). This would suggest that either the affinity is low, or the affinity is high and there are only a limited number of binding sites available for Int. Our data points to the latter explanation; IntPeri-MBP does not bind to chitin, which suggests to us that the PGN carbohydrate backbone alone is not the target of the Int LysM domain, but that some particular muropeptide or combination of crosslinked PGN strands is required for binding. The dimerisation of the LysM may have something to do with the specific binding: it could either position the two PGN binding sites of the dimer in such a way that the protein can optimally interact with the specifically crosslinked strands, or dimerisation increases the affinity of the dimer for PGN. In contrast to inverse autotransporters, many PGN-binding proteins contain several LysMs in tandem (Buist *et al.*, 2008). Dimerisation may thus be a mechanism to increase the number of PGN binding units and thereby the strength of the interaction. We are now pursuing further characterisation of the binding determinants for the Int periplasmic domain in PGN.

***The dimerisation interface(s)***

We demonstrate here that the Int periplasmic domain is a dimerisation interface for Int. This is in contrast to a previous report implicating the β-barrel domain as the dimerisation interface (Touzé *et al.*, 2004). However, Fairman *et al*. have shown that the β-barrel alone does not dimerise (Fairman *et al.*, 2012), which suggests that the dimerisation is mediated by the regions immediately upstream or downstream of the β-barrel domain. We tested whether the N-terminal Ig-like D00 domain forms dimers, but our SEC experiments show that it does not. Therefore, the dimerisation observed by Touzé *et al*. is probably due to the C-terminal helix (Helix2) of the periplasmic domain. However, this region of the periplasmic domain does not mediate dimerisation when fused N-terminally to MBP. A likely explanation for this discrepancy is that Helix2 is intimately connected to the β-barrel domain, and therefore protease-resistant, as shown by Touzé *et al.* (2004). When fused to MBP, these connections

are lost and the helix remains either unfolded or misfolded and thus cannot mediate dimerisation. This finding is supported by the observation that both IntPeri-MBP and IntHelix2-MBP were prone to degradation.

We also observed clear dimerisation by the LysM region alone, a finding has not been reported before. Both the full periplasmic domain and the N-terminal, LysM-containing region mediated dimerisation in SEC experiments when fused to MBP. A notable feature of these experiments was that the dimeric form was in equilibrium with the monomeric form. This is in contrast to the findings of Touzé *et al.*, who only observed obligate dimerisation of Int.

Though our SEC experiments show clear evidence for the N-terminal region of IntPeri mediating dimerisation, unfortunately we did not observe dimers when solving the solution structure. This is most likely due to the unfolding of the C-terminal spacer element upstream of the LysM. This region may require a C-terminal anchor (Helix1 under native condition, or MBP in our constructs) to fold stably. The instability of this region outside its native context could explain why we saw an equilibrium between the dimeric and monomeric states in SEC. We thus conclude that it is not the LysM itself that is the dimerisation interface, but the upstream sequence. This conclusion is supported by the fact that YrInvPeri forms disulphide-bonded tetramers. The single cysteine in the periplasmic domain is located in the spacer sequence, suggesting that this region is in fact the dimerisation (or oligomerisation) interface. That the periplasmic domain of YrInv also mediates oligomerisation suggests that oligomer formation is a general feature of LysM-containing inverse autotransporters. In the case of YrInv, the physiological relevance of the disulphide-bonded tetramer remains to be determined.

In conclusion, we present a new model for Int dimerisation, where the LysM of the periplasmic domain is the dimerisation interface, with two sites for dimer formation: Helix2 and the spacer sequence between the LysM and Helix1 (Fig. 9). This is a modification of the earlier model of Touzé *et al.* (2004), which suggested that a single Int dimer interacts with two separate Tir dimers, leading to a reticular array of Int-Tir interactions and receptor clustering. This is consistent with the crystal structure of Int-Tir, where the Int monomers jut out from the Tir dimer in opposite directions (Fig. 8) (Luo *et al.*, 2000).

***Biological implications***

What might be the function of PGN binding in a subset of inverse autotransporters? One possibility might be to anchor the protein to specific sites in PGN and thus prevent lateral diffusion in the outer membrane. This could be useful for A/E pathogens, such as EPEC, for pedestal formation and in

maintaining intimate attachment to host cells. Another interesting facet of the Int-PGN interaction is the dependence on low pH, which appears to be a conserved feature based on our results with YrInv. The pH dependence of inverse autotransporter LysM binding suggests that charged residues are involved in binding. IntPeri has a calculated isoelectric point (pI) of 8.7, and YrInvPeri has a pI of 6.1. Thus, at pH 5.0, both proteins carry a net positive charge which may play a role in PGN binding. A similar result was obtained for AcmD, an autolysin from *Lactococcus lactis* containing three LysMs, where binding to the cell wall was only detected below the pI of the protein (Visweswaran *et al.*, 2013). Interestingly, Int is upregulated under acid stress (House *et al.*, 2009). As EPEC and other A/E pathogens must travel through the stomach to reach the intestine, and the pH of the periplasm closely follows the pH of the extracellular medium (Wilks and Slonczewski, 2007), the periplasm will experience a significant drop in pH during the pathogen's journey through the stomach. The binding to PGN may help in stabilising the cell envelope and aid in acid resistance; however, our attempts to probe the acid resistance of Int-expressing bacteria using survival assays did not yield any conclusive results compared to control cells (data not shown).

The function of PGN binding and dimerisation remain unclear. The model proposed by Touzé *et al.* (2004) suggests that Int dimerisation leads to more efficient Tir clustering on the host cell membrane and the initiation of downstream effects. Purified Int passenger domain can also lead to actin rearrangements (Liu *et al.*, 1999), but these experiments were carried out using a GST fusion, and GST forms dimers, which could explain this observation. Bacteria expressing periplasmically truncated Int or InvPeri-Int did not bind as strongly to HeLa cells as wt Int, possibly due to less surface exposure of the protein in the case of IntΔPeri, but potentially as a result of the loss of dimer formation in the case of the chimaeric protein. Interestingly, a recent study showed that an Inv-Int fusion that binds to Tir failed to form actin pedestals when expressed in *Citrobacter rodentium*, and that this strain was defective in colonising a mouse model (Mallick *et al.*, 2012). As this fusion lacks a dimerisation interface, it is tempting to speculate that the defects are at least partially due to the protein not forming a functional dimer. Dimerisation seems to be important for inverse autotransporter function, as it is widely conserved within the protein family. In contrast to LysM-containing inverse autotransporters, Inv from *Y. pseudotuberculosis* forms dimers and tetramers, but in the absence of a LysM (Dersch and Isberg, 1999). The multimerisation interface is in the D2 Ig-like domain in the passenger region, which is missing in the *Y. enterocolitica* orthologue (Dersch and Isberg, 2000). The *Y. pseudotuberculosis* protein is the more potent invasin and promotes a stronger cellular response compared to *Y. enterocolitica* Inv, presumably

due to receptor clustering (Dersch and Isberg, 2000). Dimerisation of inverse autotransporters thus appears functionally important and can occur through at least two distinct mechanisms: through dimerisation of the periplasmic domain or by self-association of domains in the passenger region.

Apart from adhesion, another aspect of the biology of type Ve-secreted adhesins in which the periplasmic domain might play a role is autotransport. Some of our data supports this hypothesis: though deletion of the entire periplasmic domain does not abolish surface display, it does reduce it. A reasonable assumption would therefore be that the conserved C-terminal helices (Helix1 and Helix2) would play a role in passenger secretion. Additionally, longer inverse autotransporters are more likely to include a LysM, which might also have a function in the autotransport process. Autotransporters of some other classes contain periplasmic domains: a few trimeric (type Vc) autotransporters contain coiled-coil periplasmic extensions, and type Vd-secreted proteins have periplasmic POTRA (polypeptide transport-associated) domains (Szczesny and Lupas, 2008; Salacha *et al.*, 2010; Arnold *et al.*, 2010). We are currently investigating the involvement of autotransporter periplasmic domains in passenger secretion.

## EXPERIMENTAL PROCEDURES

### *Bioinformatic analyses*

To identify periplasmic domains of inverse autotransporters, we performed a PSI-BLAST (Altschul and Koonin, 1998) search with 5 iterations against the non-redundant database using either the Int or Inv periplasmic domain and β-barrel domain sequence. We included the latter to correctly identify type Ve-secreted proteins, and only hits covering over 80% of the query (so as to contain sequence from both the β-barrel and periplasmic domain) were included. The search results were pooled and duplicate hits removed. The sequences were then checked manually and any clearly false positive results (*i.e*. those lacking the β-barrel domain) were removed. The remaining sequences (many of which appear to misannotated in the database) were aligned and the β-barrel domains removed based on the alignment. To identify signal peptide cleavage sites, we submitted the sequences to SignalP 4.0 (Petersen *et al.*, 2011) or Phobius (Käll *et al.*, 2004), and the sequence N-terminal to the consensus cleavage site were removed. The remaining sequences were then checked for the presence of a LysM motif using HHPred (Söding *et al.*, 2005). For clustering, we used CLANS (Frickey and Lupas, 2004) with default parameter values. Alignments and secondary structure analysis were performed using programmes in the MPI Bioinformatics Toolkit (Biegert *et al.*, 2006)(http://toolkit.tuebingen.mpg.de/).

***Cloning***

We amplified the regions of interest from genomic DNA of *E. coli* O127:H6 strain 2348/69 (for Int), *Y. enterocolitica* O:8 strain 8081 (for Inv) or *Y. ruckeri* strain CECT 4319 (for YrInv) using polymerase chain reaction (PCR) with Phusion polymerase (Thermo Scientific). Primers were constructed to include N- and C-terminal BsaI sites for cloning into vectors of the pASK-IBA series (IBA GmbH). For the periplasmic domains, primers were designed to introduce an N-terminal hexahistidine tag for protein purification. Primer sequences are available on request. Constructs used in this study are summarised in Table 1. For producing MBP fusions, we introduced in-frame BamHI and NheI restriction sites after the 3' end of the insert by PCR-based site-directed mutagenesis (Byrappa *et al.*, 1995). The MBP coding sequence was amplified from the plasmid pMal-c2 (New England Biolabs) with primers that introduced BamHI and NheI sites to the 5' and 3'-ends, respectively. This product was then cloned into the corresponding sites in the modified pIBA-ASK plasmids to produce the final fusion construct. For fusion controls, we amplified MBP with primers introducing BsaI sites and cloned the PCR product into pASK-IBA33 to include a C-terminal hexahistidine tag for efficient purification. To purify Int LysM alone, we amplified the IntLysM-MBP insert from pIBA2-IntPeriLysM-MBP with the forward primer lacking the His tag sequence. This product was then cloned into pASK-IBA33 to introduce a C-terminal His tag on the MBP moiety, and a TEV site was introduced between the LysM and MBP by site-directed mutagenesis. To produce domain-swapped Inv and Int constructs, we performed a two-step PCR reaction, where the primers at the fusion junction where designed to overlap (Barik, 1997). Restriction enzymes were from New England Biolabs, and T4 DNA ligase from Fermentas.

***Bacterial strains and growth media***

For cloning, all ligation reactions were transformed into chemically competent *E. coli* TOP10 (Invitrogen). For protein overproduction in the cytoplasm, we used the expression strain BL21Gold(DE3) (Novagen). For surface production, the BL21 derivative strain omp2 was used, which is optimised for outer membrane protein expression (Prilipov *et al.*, 1998). Bacteria were usually grown in lysogeny broth medium (LB) (Bertani, 1951) supplemented with ampicillin (100 μg/ml) or chloramphenicol (25 μg/ml). For protein production, we used the buffered, rich medium ZYP (Studier, 2005) supplemented with ampicillin as above.

***Protein production and purification***

For production of MBP and MBP fusions, an overnight culture of BL21Gold transformed with the required plasmid was diluted 1:100 in 1 l ZYP medium and grown to mid-log phase ($OD_{600}$~0.5) at 37 °C, at which time protein production was induced with anhydrotetracycline (200 ng/ml).The cultures were then grown for another 3 hours at 37 °C after which the cells were harvested by centrifuging (10 minutes 5000 x *g*) and then resuspended in Ni binding buffer (20 mM sodium phosphate, 20 mM imidazole, 500 mM sodium chloride, pH 7.4). We added $MgCl_2$ and $MnCl_2$ to 1 mM, lysozyme to 0.1 mg/ml, EDTA-free complete protease inhibitor cocktail (Roche) and a pinch of DNase I (Applichem) and proceeded to rupture the cells using a French pressure cell with two passes at 18 000 p.s.i. Cellular debris were pelleted for 1 hour at 100 000 x *g*, the supernatant was passed through a 0.22 µm filter and applied to a nickel iminodiacetic acid column (PrepEase; USB). Bound proteins were eluted with a step gradient of imidazole (250 mM) in Ni binding buffer. We pooled the fractions containing the periplasmic domain-MBP fusions, added protease inhibitor cocktail and applied these to an amylose column (MBPTrap; GE Healthcare) equilibrated with 20 mM Tris, 200 mM NaCl, 1 mM EDTA at pH 7.4. Bound protein was eluted using the same buffer supplemented with 10 mM maltose. Proteins were further purified by size exclusion chromatography (Superdex200™ 26/60 column; GE Healthcare) in Tris-buffered saline (TBS; 20 mM Tris pH 7.4 with 150 mM NaCl and 0.02% $NaN_3$).

For producing isotope-labeled protein for NMR experiments, we grew cells overnight in minimal medium M9 (Hochuli *et al.*, 2000) supplemented with 1% LB and ampicillin at 100 µg/ml. The cultures were then diluted 1:200 in 2 l of M9 + 1% LB + ampicillin containing $^{15}NH_3Cl$ and $^{13}C$-glucose (Sigma). Once the cultures reached mid-log phase, protein production was induced and the cultures were harvested after 3 hours at 37 °C. The cells were resuspended in Ni binding buffer and lysed as above. After passing over a nickel column, the eluted protein was dialysed overnight against phosphate-buffered saline (PBS; 20 mM phosphate pH 7.4, 150 mM NaCl). The following morning, TEV protease (produced according to (Tropea *et al.*, 2009) was added to 1/10 of the concentration of sample protein as estimated by absorbance at 280 nm. The digestion was allowed to proceed for 4 hours at room temperature, after which the digested protein was passed over the nickel column again. The flow through contained the digested, labeled protein. This was further purified by size exclusion chromatography using a Superdex75$^{TM}$ 16/60 column (GE Healthcare) equilibrated with PBS.

For outer membrane expression, overnight cultures were diluted 1:100 in 20 ml ZYP medium and grown till mid-log phase at 37 °C. The temperature was then adjusted to 27 °C and protein production was

induced with anhydrotetracycline (50 ng/ml). The cells were grown for approximately two hours at 27 °C before harvesting.

***NMR structure determination***

All spectra were recorded at 298 K on Bruker AVIII-600 and AVIII-800 spectrometers. Backbone sequential assignments were completed using a strategy based on a 3D-HN(CA)NNH experiment (Weisemann *et al.*, 1993). Aliphatic sidechain assignments were completed with standard TOCSY-based experiments, while aromatic assignments were made by linking aromatic spin systems to the respective $C^{\beta}H_2$ protons in a 2D-NOESY spectrum. Stereospecific assignments and the resulting $\chi 1$ rotamer assignments were determined from a combination of HNHB and HA[HBHN](CACO)NH experiments (Löhr *et al.*, 1999).

Distance data were derived from a set of five 3D-NOESY spectra, including the heteronuclear edited NNH-, CCH-, and CNH-NOESY spectra (Diercks *et al.*, 1999) in addition to conventional $^{15}N$- and $^{13}C$-HSQC-NOESY spectra. A $^{12}C$-filtered 2D-NOESY spectrum was recorded for the observation of contacts to aromatic groups. Backbone dihedral angle restraints were derived using the TALOS+ server (Shen *et al.*, 2009). Generic backbone dihedral restraints designed to restrict residues to allowed regions of the Ramachandran map and well-populated sidechain rotamers were applied for unstructured residues. Hydrogen bond restraints were applied as pseudo-covalent bonds, as outlined in (Truffault *et al.*, 2001). Refinement was carried out by comparing experimental and back-calculated NOESY spectra using in-house software. Strips were back calculated for the amide protons of all ordered atoms, plus selected sidechain groups. These were compared to the experimental spectra to confirm backbone and sidechain dihedral angles and to extract additional distance restraints.

Structures were calcuated with XPLOR (NIH version 2.9.4) using standard protocols with modifications for the inclusion of H-bonds as pseudo-covalent bonds. For the final set, 100 structures were calculated and 18 chosen on the basis of lowest restraint violations. An average structure was calculated and regularized to give a structure representative of the ensemble. Details of the input data and the final ensemble are given in Table S2.

***Surface display and functional controls***

Immunofluorescence microscopy, FACS, pre-infection adhesion assays and ELISA for IL-8 production were all performed as described (Oberhettinger *et al.*, 2012).

***Analytical size exclusion chromatography***

Gel sizing was done using a Superdex™200 10/300 column (GE Healthcare) equilibrated either with TBS or acetate-buffered saline (ABS; 20 mM sodium acetate pH 4.0 with 150 mM NaCl). Approximately 1 mg of protein was applied to the column, and elution was monitored by absorbance at 280 nm. For sizing, a preparation of standard proteins (Ribonuclease A (13.7 kDa), Conalbumin (75 kDa), Aldolase (158 kDa), Ferritin (440 kDa) from GE Healthcare) was passed through the column. We then compared the position of the sample proteins' peaks to a standard curve drawn based on the elution profile of the standard mix to obtain apparent molecular weights.

***Peptidoglycan and chitin binding***

Peptidoglycan sacculi from *E. coli* Nissle were purified according to the method of Glauner with some modifications (Glauner, 1988). The lyophilized sacculi were resuspended in ultrapure water (with sodium azide added to 0.02% w/v) to a concentration of 10 mg/ml. For pull-down assays, 2 μl of this suspension was mixed with 5 μg of protein in a total volume of 30 μl and incubated for 15 minutes at room temperature. The buffer used depended on the pH: we used TBS (pH 8.0 or pH 7.4), MOPS-buffered saline (pH 7.0), MES-buffered saline (pH 6.0), ABS (pH 5.0 and pH 4.0) or glycine-buffered saline (pH 3.0). The sacculi were then pelleted by centrifuging 30 minutes at ~20 000 x *g* (full speed using a tabletop centrifuge). The supernatant was carefully removed and the pellet was washed once with the corresponding buffer. After a second centrifugation step the supernatant was removed and the pellet was resuspended in 30 μl TBS (pH 7.4). For analysis, we added 10 μl of 4X non-reducing sample buffer to the first supernatant fraction and the pellet fraction, boiled the samples for 5 minutes and then loaded 10 μl onto a 12% polyacrylamide gel for SDS-PAGE.

For competition experiments, 20 mg of *E. coli* PGN sacculi were digested with mutanolysin (4000 U; from Sigma) in a total volume of 800 μl PBS for 16 hours at 37 °C. After heat inactivation of the enzyme (100 °C, 2 min), the undigested PGN was pelleted (30 min at ~20 000 x *g*) and the supernatant was transferred to a new tube. The pH of the solution was changed to 5.0 by the addition of 50 μl 1 M NaAc at this pH; the pH of the solution was checked after mixing. An estimated 30-40% of the sacculi were digested, giving a concentration of ~7 mg/ml of various muropeptides. We used 5, 10, 15, 20 or 25 μl of the muropeptide solution in our competition experiment. The muropeptides and IntPeri-MBP (5 μg as above) were mixed first, and peptidoglycan sacculi were subsequently added. The total volume was adjusted to 30 μl with ABS pH 5.0. The procedure from this point on was as above.

For the concentration series, we varied the amount of protein between 0.5 μg and 10 μg. The amount of peptidoglycan was varied between 2 μg to 50 μg. The binding buffer was ABS (pH 5.0). The samples were otherwise treated as above.

Chitin binding was assayed using chitin beads (New England Biolabs). We prepared columns using 2 ml of the bead slurry and equilibrated with ABS (pH 5.0). We added 1 mg of protein diluted in 1 ml of ABS and allowed the protein to enter the column by gravity flow. After washing with 10 ml ABS, bound protein was eluted with 10 ml TBS (pH 7.4), followed by a second elution step with 0.3 M NaOH. A sample was taken from each step for SDS-PAGE analysis.

**In vivo *PGN binding***

To test for PGN binding in whole cells, we transformed the plasmids pIBA2C-IntPeri-MBP, pIBA2C-InvPeri-MBP or pASK-IBA2C into BL21omp2 cells. The cells were then grown at 37 °C in LB + chloramphenicol (25 μg/ml) till mid-log, at which time the temperature was changed to 27 °C. Growth at this temperature in the presence of maltose leads to expression of endogenous MBP in BL21 and its derivatives (REF). After 30 minutes, recombinant protein production was induced with AHTC (50 ng/ml). After 1 hour at 27 °C, we added buffer, either Tris pH 7.4 or sodium acetate pH 5.5, to 100 mM. After a further hour of growth the turbidity of the cultures ($OD_{600}$) was measured and an amount of cells corresponding to 10 ml at an $OD_{600}$ value of 1.0 was harvested by centrifugation (10 minutes 3500 x *g*). To examine the soluble periplasmic fraction, we used a modified osmotic shock protocol. The pelleted cells were resuspended in 400 μl 5 mM $CaCl_2$ with 5 mM buffer (Tris pH 7.4 or sodium acetate pH 5.5) and incubated on ice for 10 minutes. This step improves the yield of the periplasmic extraction (Chen *et al.*, 2004). The cells were pelleted (5 minutes at 8000 x *g*) and then resuspended in 400 μl ice-cold osmotic shock solution (33 mM buffer, 20 % sucrose, 5 mM EDTA) buffered at either pH 7.4 or pH 5.5, as above. After 10 minutes incubation at 8 °C with shaking, the cells were centrifuged as above and then resuspended in 400 μl 5 mM buffer (either Tris pH 7.4 or sodium acetate pH 5.5). The cells were incubated for 10 minutes with shaking at 8 °C and then centrifuged as above. A sample (120 μl) was taken from the supernatant, and 40 μl 4 x SDS-PAGE sample buffer was added. This represented the periplasmic fraction. For the whole-cell sample, we pelleted an amount of cells from the induced culture corresponding to 120 μl at $OD_{600}$ = 25, resuspended these in 120 μl PBS and then added 40 μl sample buffer.

To probe for the recombinant proteins, we performed a Western blot. The proteins were separated in a 10% polyacrylamide gel and then transferred to a nitrocellulose membrane (Protran BA 85, GE Healthcare) using a semi-dry apparatus. The membrane was blocked for 30 minutes with 5% fat-free milk powder in TBS. The primary antibody was a rabbit anti-MBP (anti-MalE) antiserum diluted in blocking buffer 1:5000. After 1 hour of blocking, the membrane was washed twice 10 minutes with TBS + 0.05% Tween20 (TBS-T), and then the secondary antibody (goat anti-rabbit-alkaline phosphatase (AP), Jackson Immunoresearch) was added at a dilution of 1:10 000 in blocking buffer. The membrane was washed twice with TBS-T as above, and a final time in AP buffer (100 mM Tris pH 9.5, 100 mM NaCl, 5 mM $MgCl_2$). Chromogenic detection was performed using the AP substrate nitro blue tetrazolium/5-bromo-4-chloro-3-indolyl phosphate (NBT/BCIP), diluted to 33 ng/ml and 17 ng/ml, respectively, in AP buffer. The reaction was stopped with deionized water once colour had developed.

The anti-MalE antiserum was obtained by immunizing a rabbit with MBP (MalE). The vaccine was prepared by emulsifying 1 mg MalE protein (denaturated with 1% SDS) with Freund's adjuvant in the cold and injected subcutaneously and intramuscularly (hind legs); after four weeks the rabbit obtained a booster injection and blood was collected with 5-6 days intervals.

***Accession numbers***

The NMR structure of the Int LysM from this publication has been submitted to the Protein Data Bank (http://www.rcsb.org/pdb) and assigned the identifier 2MPW.

## Author contributions

J.C.L., P.O., M.S., Mu.Co., I.B.A. and D.L. designed and J.C.L., P.O., Ma.Ch., and Mu.Co. performed the experiments and analysed the data. D.K., U.B., H.S. and F.G. provided essential materials. J.C.L., P.O. and D.L. wrote the paper.

## Acknowledgments

We would like to thank M.Sc. Iwan Grin (MPI for Develepmental Biology, Tübingen) for assistance with parsing the sequences for bioinformatic analyses. We are also grateful to Dr. Jörg Rau (Chemisches und Veterinäruntersuchungsamt, Stuttgart) for providing the *Y. ruckeri* DNA. We thank Prof. Andrei Lupas (Protein Evolution, MPI for Developmental Biology, Tübingen) for continued support. This study was

631 funded by the Sonderforschungsbereich 766 of the DFG (German Science Foundation) to D.L., I.B.A., U.B.
632 and F.G., UKT fortüne F1433253 to P.O., and a FEMS Advanced Fellowship to J.C.L.

633 **REFERENCES**

634 Altschul, S.F., and Koonin, E.V. (1998) Iterated profile searches with PSI-BLAST--a tool for discovery in
635 protein databases. *Trends Biochem Scis* **23**: 444-7.

636 Arnold, T., Zeth, K., and Linke, D. (2010) Omp85 from the thermophilic cyanobacterium
637 *Thermosynechococcus elongatus* differs from proteobacterial Omp85 in structure and domain
638 composition. *J Biol Chem* **285**: 18003-15.

639 Barik, S. (1997) Mutagenesis and gene fusion by megaprimer PCR. *Methods Mol Biol (Clifton, N.J.)* **67**:
640 173-82.

641 Bateman, A., and Bycroft, M. (2000) The structure of a LysM domain from *E. coli* membrane-bound lytic
642 murein transglycosylase D (MltD). *J Mol Biol* **299**: 1113-9.

643 Bertani, G. (1951) Studies on lysogenesis. I. The mode of phage liberation by lysogenic *Escherichia coli*. *J*
644 *Bacteriol* **62**: 293-300.

645 Biegert, A., Mayer, C., Remmert, M., Söding, J., and Lupas, A.N. (2006) The MPI Bioinformatics Toolkit for
646 protein sequence analysis. *Nucleic Acids Res* **34**: W335-9.

647 Bielnicki, J., Devedjiev, Y., Derewenda, U., Dauter, Z., Joachimiak, A., and Derewenda, Z.S. (2006) *B.*
648 *subtilis* ykuD protein at 2.0 A resolution: insights into the structure and function of a novel, ubiquitous
649 family of bacterial enzymes. *Proteins* **62**: 144-51.

650 Buist, G., Steen, A., Kok, J., and Kuipers, O. (2008) LysM, a widely distributed protein motif for binding to
651 (peptido)glycans. *Mol Microbiol* **68**: 838-47.

652 Byrappa, S., Gavin, D.K., and Gupta, K.C. (1995) A highly efficient procedure for site-specific mutagenesis
653 of full-length plasmids using Vent DNA polymerase. *Genome Res* **5**: 1-5.

654 Chen, Y., Chen, L., Chen, S., Chang, M., and Chen, T. (2004) A modified osmotic shock for periplasmic
655 release of a recombinant creatinase from *Escherichia coli*. *Biochem Eng J* **19**: 211-215.

656 Dersch, P., and Isberg, R.R. (1999) A region of the *Yersinia pseudotuberculosis* invasin protein enhances
657 integrin-mediated uptake into mammalian cells and promotes self-association. *EMBO J* **18**: 1199-213.

658 Dersch, P., and Isberg, R.R. (2000) An immunoglobulin superfamily-like domain unique to the *Yersinia*
659 *pseudotuberculosis* invasin protein is required for stimulation of bacterial uptake via integrin receptors.
660 *Infect Immun* **68**: 2930-8.

661 Diercks, T., Coles, M., and Kessler, H. (1999) An efficient strategy for assignment of cross-peaks in 3D
662 heteronuclear NOESY experiments. *J Biomol NMR* **15**: 177-80.

663 Fairman, J.W., Dautin, N., Wojtowicz, D., Liu, W., Noinaj, N., Barnard, T.J., *et al.* (2012) Crystal structures
664 of the outer membrane domain of intimin and invasin from enterohemorrhagic *E. coli* and
665 enteropathogenic *Y. pseudotuberculosis*. *Structure* **20**: 1233-43.

666 Frickey, T., and Lupas, A. (2004) CLANS: a Java application for visualizing protein families based on
667 pairwise similarity. *Bioinformatics (Oxford, England)* **20**: 3702-4.

668 Glauner, B. (1988) Separation and quantification of muropeptides with high-performance liquid
669 chromatography. *Anal Biochem* **172**: 451-64.

670 Hamburger, Z.A., Brown, M.S., Isberg, R.R., and Bjorkman, P.J. (1999) Crystal structure of invasin: a
671 bacterial integrin-binding protein. *Science (New York, N.Y.)* **286**: 291-5.

672 Hochuli, M., Szyperski, T., and Wüthrich, K. (2000) Deuterium isotope effects on the central carbon
673 metabolism of Escherichia coli cells grown on a D2O-containing minimal medium. *J Biomol NMR* **17**: 33-
674 42.

675 House, B., Kus, J.V., Prayitno, N., Mair, R., Que, L., Chingcuanco, F., *et al.* (2009) Acid-stress-induced
676 changes in enterohaemorrhagic *Escherichia coli* O157:H7 virulence. *Microbiology (Reading, England)*
677 **155**: 2907-18.

678 Humphrey, W., Dalke, A., and Schulten, K. (1996) VMD: visual molecular dynamics. *J Molecular Graph*
679 **14**: 33-8, 27-8.

680 Kelly, G., Prasannan, S., Daniell, S., Fleming, K., Frankel, G., Dougan, G., *et al.* (1999) Structure of the cell-
681 adhesion fragment of intimin from enteropathogenic *Escherichia coli*. *Nat Struct Biol* **6**: 313-8.

682 Käll, L., Krogh, A., and Sonnhammer, E.L. (2004) A combined transmembrane topology and signal
683 peptide prediction method. *J Mol Biol* **338**: 1027-36.

684 Leo, J.C., Grin, I., and Linke, D. (2012) Type V secretion: mechanism(s) of autotransport through the
685 bacterial outer membrane. *Philos Trans R Soc Lond, B, Biol Sci* **367**: 1088-1101.

686 Leo, J.C., and Skurnik, M. (2011) Adhesins of human pathogens from the genus *Yersinia*. *Adv Exp Med*
687 *Biol* **715**: 1-15.

688 Leong, J.M., Fournier, R.S., and Isberg, R.R. (1990) Identification of the integrin binding domain of the
689 *Yersinia pseudotuberculosis* invasin protein. *EMBO J* **9**: 1979-89.

690 Liu, H., Magoun, L., Luperchio, S., Schauer, D., and Leong, J. (1999) The Tir-binding region of
691 enterohaemorrhagic *Escherichia coli* intimin is sufficient to trigger actin condensation after bacterial-
692 induced host cell signalling. *Mol Microbiol* **34**: 67-81.

693 Luo, Y., Frey, E.A., Pfuetzner, R.A., Creagh, A.L., Knoechel, D.G., Haynes, C.A., *et al.* (2000) Crystal
694 structure of enteropathogenic *Escherichia coli* intimin-receptor complex. *Nature* **405**: 1073-7.

695 Löhr, F., Schmidt, J.M., and Rüterjans, H. (1999) Simultaneous Measurement of $^{3}J_{HN,H\alpha}$ and $^{3}J_{H\alpha,H\beta}$ Coupling
696 Constants in $^{13}C$,$^{15}N$-Labeled Proteins. *J Am Chem Soc* **121**: 11821-11826.

697 Mallick, E.M., Brady, M.J., Luperchio, S.A., Vanguri, V.K., Magoun, L., Liu, H., *et al.* (2012) Allele- and Tir-
698 independent functions of intimin in diverse animal infection models. *Front Microbiol* **3**: 11.

699 Maxwell, K.L., Hassanabad, M.F., Chang, T., Pirani, N., Bona, D., Edwards, A.M., and Davidson, A.R.
700 (2013) Structural and functional studies of gpX of *Escherichia coli* phage P2 reveal a widespread role for
701 LysM domains in the baseplates of contractile-tailed phages. *J Bacteriol* **195**: 5461-8.

702 Oberhettinger, P., Schütz, M., Leo, J.C., Heinz, N., Berger, J., Autenrieth, I.B., and Linke, D. (2012) Intimin
703 and invasin export their C-terminus to the bacterial cell surface using an inverse mechanism compared
704 to classical autotransport. *PLoS ONE* **7**: e47069.

705 Petersen, T.N., Brunak, S., Heijne, von, G., and Nielsen, H. (2011) SignalP 4.0: discriminating signal
706 peptides from transmembrane regions. *Nat Methods* **8**: 785-6.

707 Pisano, F., Kochut, A., Uliczka, F., Geyer, R., Stolz, T., Thiermann, T., *et al.* (2012) *In vivo*-induced InvA-like
708 autotransporters Ifp and InvC of *Yersinia pseudotuberculosis* promote interactions with intestinal
709 epithelial cells and contribute to virulence. *Infect Immun* **80**: 1050-64.

710 Prilipov, A., Phale, P.S., van Gelder, P., Rosenbusch, J.P., and Koebnik, R. (1998) Coupling site-directed
711 mutagenesis with high-level expression: large scale production of mutant porins from *E. coli*. *FEMS*
712 *Microbiol Lett* **163**: 65-72.

713 Quintela, J.C., Caparrós, M., and de Pedro, M.A. (1995) Variability of peptidoglycan structural
714 parameters in gram-negative bacteria. *FEMS Microbiol Lett* **125**: 95-100.

715 Salacha, R., Kovacić, F., Brochier-Armanet, C., Wilhelm, S., Tommassen, J., Filloux, A., *et al.* (2010) The
716 *Pseudomonas aeruginosa* patatin-like protein PlpD is the archetype of a novel Type V secretion system.
717 *Environ Microbiol* **12**: 1498-512.

718 Schmidt, M.A. (2010) LEEways: tales of EPEC, ATEC and EHEC. *Cell Microbiol* **12**: 1544-52.

719 Schneider, C.A., Rasband, W.S., and Eliceiri, K.W. (2012) NIH Image to ImageJ: 25 years of image analysis.
720 *Nat Methods* **9**: 671-5.

721 Shen, Y., Delaglio, F., Cornilescu, G., and Bax, A. (2009) TALOS+: a hybrid method for predicting protein
722 backbone torsion angles from NMR chemical shifts. *J Biomol NMR* **44**: 213-23.

723 Studier, F.W. (2005) Protein production by auto-induction in high density shaking cultures. *Protein Expr*
724 *Purif* **41**: 207-34.

Szczesny, P., and Lupas, A. (2008) Domain annotation of trimeric autotransporter adhesins--daTAA. *Bioinformatics (Oxford, England)* **24**: 1251-6.

Söding, J., Biegert, A., and Lupas, A.N. (2005) The HHpred interactive server for protein homology detection and structure prediction. *Nucleic Acids Res* **33**: W244-8.

Touzé, T., Hayward, R.D., Eswaran, J., Leong, J.M., and Koronakis, V. (2004) Self-association of EPEC intimin mediated by the β-barrel-containing anchor domain: a role in clustering of the Tir receptor. *Mol Microbiol* **51**: 73-87.

Tropea, J.E., Cherry, S., and Waugh, D.S. (2009) Expression and purification of soluble His(6)-tagged TEV protease. *Methods Mol Biol (Clifton, N.J.)* **498**: 297-307.

Truffault, V., Coles, M., Diercks, T., Abelmann, K., Eberhardt, S., Lüttgen, H., *et al.* (2001) The solution structure of the N-terminal domain of riboflavin synthase. *J Mol Biol* **309**: 949-60.

Tsai, J.C., Yen, M., Castillo, R., Leyton, D.L., Henderson, I.R., and Saier, M.H. (2010) The bacterial intimins and invasins: a large and novel family of secreted proteins. *PLoS ONE* **5**: e14403-14.

Visweswaran, G.R.R., Steen, A., Leenhouts, K., Szeliga, M., Ruban, B., Hesseling-Meinders, A., *et al.* (2013) AcmD, a homolog of the major autolysin AcmA *of Lactococcus lactis*, binds to the cell wall and contributes to cell separation and autolysis. *PLoS ONE* **8**: e72167.

Weisemann, R., Rüterjans, H., and Bermel, W. (1993) 3D triple-resonance NMR techniques for the sequential assignment of NH and 15N resonances in 15N- and 13C-labelled proteins. *J Biomol NMR* **3**: 113-20.

Wilks, J.C., and Slonczewski, J.L. (2007) pH of the cytoplasm and periplasm of *Escherichia coli*: rapid measurement by green fluorescent protein fluorimetry. *J Bacteriol* **189**: 5601-7.

747 **TABLES**

748 **Table 1**. Plasmids used in this study.

| Plasmid | Insert sequence | Vector | Comment | Reference/source |
|---|---|---|---|---|
| pASK-IBA2 | - | pASK-IBA2 | Expression vector with N-terminal OmpA signal peptide for periplasmic targeting, with ampicillin resistance. | IBA GmbH |
| pASK-IBA2C | - | pASK-IBA2C | Expression vector with N-terminal OmpA signal peptide for periplasmic targeting, with chloramphenicol resistance. | IBA GmbH |
| pASK-IBA3 | - | pASK-IBA3 | Expression vector for cytoplasmic expression. | IBA GmbH |
| pASK-IBA33 | - | pASK-IBA33 | Expression vector for cytoplasmic expression, with C-terminal His tag. | IBA GmbH |
| pIBA2C-IntPeri-MPB | Int periplasmic domain (residues 40-212) | pASK-IBA2C | Produces IntPeri with a C-terminal MBP fusion; includes N-terminal signal peptide for periplasmic transport. | This study |
| pIBA2C-InvPeri-MBP | Inv periplasmic domain (residues 35-93) | pASK-IBA2C | Produces InvPeri with a C-terminal MBP fusion; includes N-terminal signal peptide for periplasmic transport. | This study |
| pIBA2C-MBP | MBP | pASK-IBA2C | Produces MBP with N-terminal signal peptide | This study |

| | | | | |
|---|---|---|---|---|
| | | | for periplasmic transport. | |
| pIBA2-IntΔLysM | Int lacking LysM domain (contains residues 144-939) | pASK-IBA2 | For production of N-terminally truncated Int at cell surface. | This study |
| pIBA2-IntΔPeri | Int lacking entire periplasmic domain (contains residues 213-939) | pASK-IBA2 | For production of N-terminally truncated Int at cell surface. | This study |
| pIBA2-IntFull | Full-length Int (without native signal peptide; residues 40-939) | pASK-IBA2 | For production of full-length Int at cell surface. | This study |
| pIBA2-IntPeriHelix1 | Int lacking LysM domain and linker to first conserved helix (contains residues 157-939) | pASK-IBA2 | For production of N-terminally truncated Int at cell surface. | This study |
| pIBA2-IntPeriHelix2 | Int lacking LysM domain and first conserved helix (residues 184-939) | pASK-IBA2 | For production of N-terminally truncated Int at cell surface | This study |
| pIBA2-InvΔPeri | Inv lacking entire periplasmic domain (residues 94-835) | pASK-IBA2 | For production of N-terminally truncated Int at cell surface. | This study |
| pIBA2-InvFull | Full-length Inv (without native signal peptide; residues 35-835) | pASK-IBA2 | For production of full-length Inv at cell surface. | This study |
| pIBA33-IntLysM-TEV-MBP | Int LysM domain (residues 40-153) | pASK-IBA33 | For production of Int LysM domain with C- | This study |

| | | | | |
|---|---|---|---|---|
| | | | terminal MBP fusion separated by TEV site. | |
| pIBA33-MBP | MBP | pASK-IBA33 | Produces MBP with a C-terminal His-tag. | This study |
| pIBA3-IntD00 | Int D00 domain (residues 450-550) | pASK-IBA3 | Produces Int N-terminal Ig-like domain | |
| pIBA3-IntLysM-MBP | Int LysM domain (residues 40-153) | pASK-IBA3 | Produces Int LysM with a C-terminal MBP fusion. | This study |
| pIBA3-IntPeriHelix1-MBP | 2 C-terminal helices of Int periplasmic domain (residues 157-212) | pASK-IBA3 | Produces conserved helices of Int periplasmic domain with a C-terminal MBP fusion. | This study |
| pIBA3-IntPeriHelix2-MBP | C-terminal helix of Int periplasmic domain (residues 184-212) | pASK-IBA3 | Produces second conserved helix of Int periplasmic domain with a C-terminal MBP fusion. | This study |
| pIBA3-IntPeri-MBP | Int periplasmic domain (residues 40-212) | pASK-IBA3 | Produces IntPeri with a C-terminal MBP fusion. | This study |
| pIBA3-InvPeri-MBP | Inv periplasmic domain (residues 35-93) | pASK-IBA3 | Produces InvPeri with a C-terminal MBP fusion. | This study |

749

750

## FIGURES AND LEGENDS

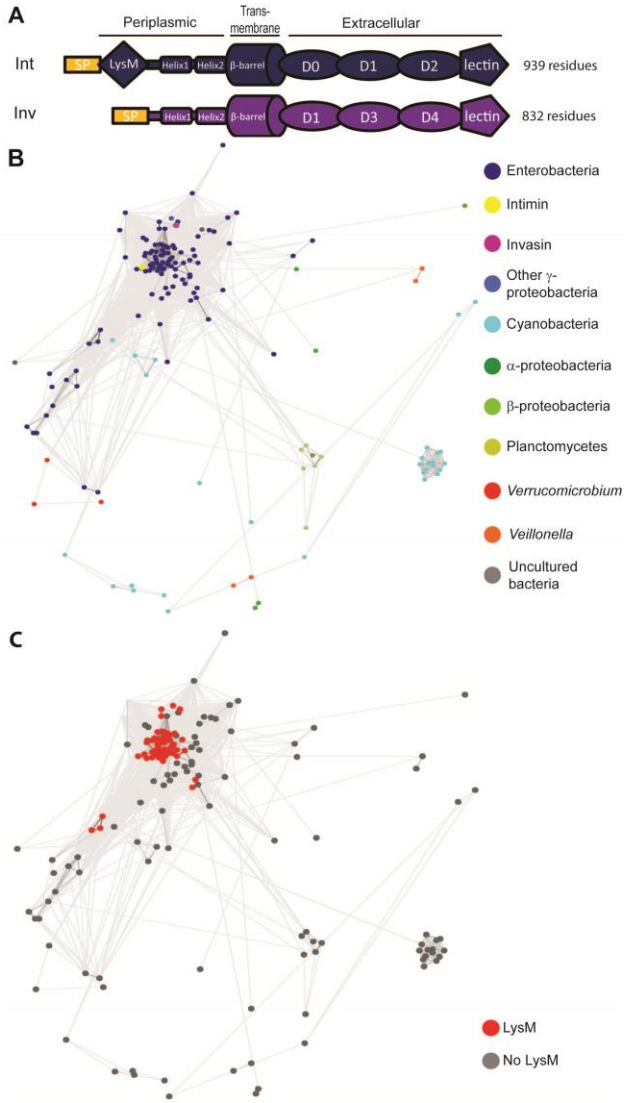


**Fig. 1.** Bioinformatic analyses of periplasmic domains of inverse autotransporters.

A. Schematic of structures of Int from EPEC (dark blue) and Inv from *Y. enterocolitica* (purple). The periplasmic domains of both contain two conserved helices (Helix1 and Helix2) at the C-terminus. In addition, the Int periplasmic domain contains a LysM, which is connected to Helix1 by a spacer sequence. SP = signal peptide. The various domains are not to scale.

B. CLANS clustering of sequences of periplasmic domains from inverse autotransporters. The sequence dots are coloured according to taxonomy. Int is indicated in yellow and Inv in magenta.

C. Highlighting of LysM-containing proteins in the cluster map from panel B. The sequences used for clustering are given is Table S1.

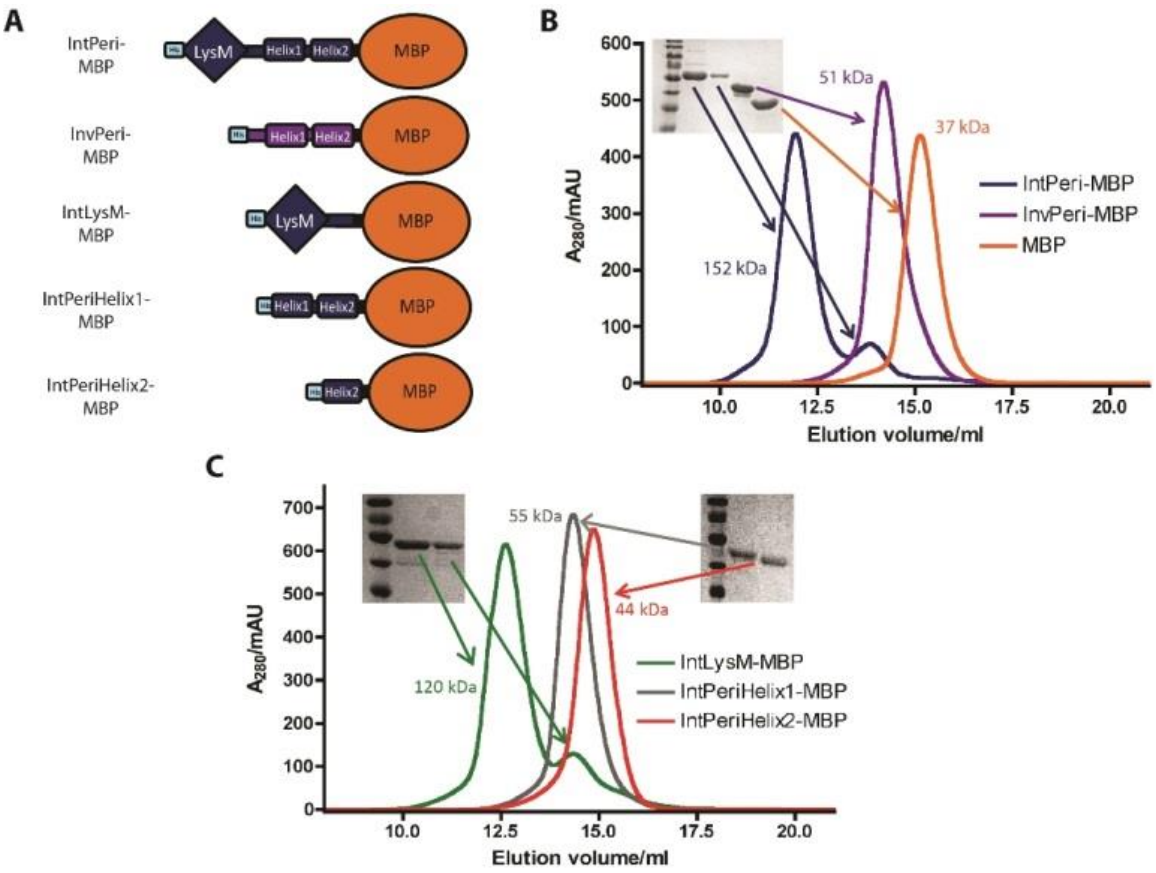


**Fig. 2.** The periplasmic domain of Int mediates dimerisation.

A. Schematic of periplasmic domain-MBP constructs. Fragments from Int are in blue, fragments from Inv in purple, MBP is in orange and the N-terminal hexahistidine tags in light blue.

B. SEC of Inv and Int periplasmic domains at pH 7.4. The curve for IntPeri-MBP is in blue, InvPeri-MBP in purple and MBP in orange. The inset shows an SDS-PAGE gel of the peaks. Apparent molecular weights of the major peaks are indicated. Expected molecular weights are 61 kDa for IntPeri-MBP, 49 kDa for InvPeri-MBP, and 41 kDa for MBP.

C: SEC of Int periplasmic domain fragments. IntLysM-MBP is in green, IntPeriHelix1-MBP in grey and IntPeriHelix2-MBP in red. The insets show SDS-PAGE gels of the peaks. Apparent molecular weights of the major peaks are indicated. Expected molecular weights are 54 kDa for IntLysM-MBP, 49 kDa for IntPeriHelix1-MBP, and 46 kDa for IntPeriHelix2-MBP.

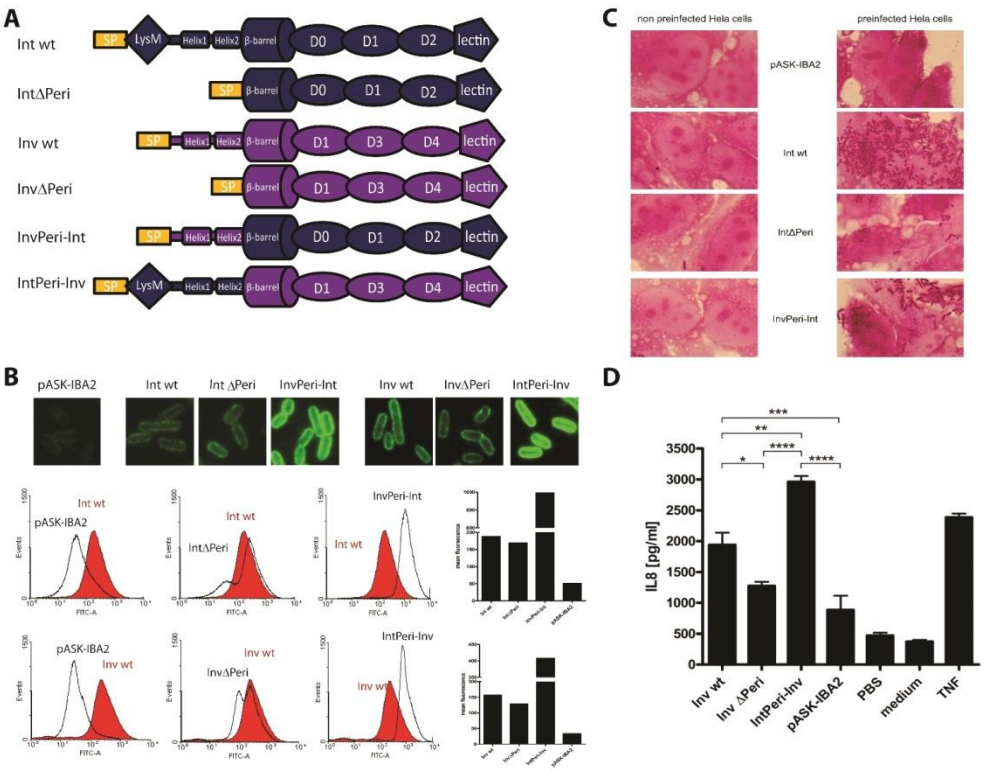


779

780 **Fig. 3.** Effect of Int and Inv periplasmic domain deletions.

781 A. Schematic of constructs used for cell surface expression experiments. In the chimaeric constructs
782 IntPeri-Inv and InvPeri-Int, the periplasmic domains of Inv and Int have been switched.

783 B. Immunofluorescence and FACS measurements for Int and Inv constructs. For the FACS
784 measurements, mean fluorescence intensity for the constructs is shown as a bar graph on the right.

785 C. Preinfection adhesion assay for Int constructs. HeLa cells were preinfected with EPEC *⊿eaeA* and then
786 incubated with *E. coli* omp2 expressing Int constructs (right-hand micrographs). Non-preinfected cells
787 and the vector pASK-IBA2 acted as negative controls.

788 D. IL-8 induction by Inv constructs. HeLa cells were incubated with *E. coli* expressing the Inv constructs
789 from panel A and IL-8 production was measured by ELISA. TNF (0.1 µg) was the positive control, PBS and
790 cell culture medium were negative controls. Error bars (S.E.M.) are from 3 replicates, stars denote
791 statistical significance as determined by ANOVA. $P < 0.05$ (*), $P < 0.01$ (**), $P < 0.001$ (***), $P < 0.0001$
792 (****).

793

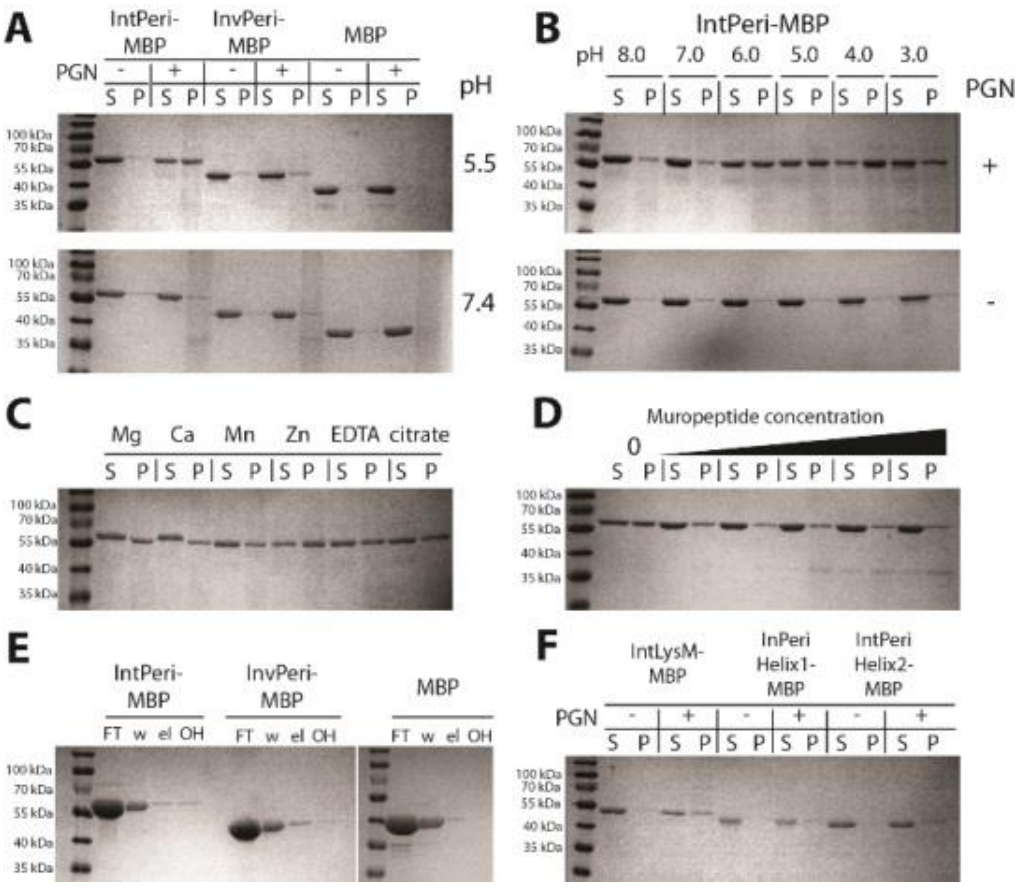


794

795 **Fig. 4.** The Int periplasmic domain binds peptidoglycan under acidic conditions

796 A. Pull-down assays using purified peptidoglycan (PGN) sacculi from *E. coli*. IntPeri-MBP, InvPeri-MBP
797 and MBP were mixed with peptidoglycan sacculi at pH 5.0 (upper gel) or pH 7.4 (lower gel) followed by
798 centrifugation. Samples were taken from the supernatant (S), and after washing, the resuspended pellet
799 (P) and separated in SDS-PAGE. Control reactions were without PGN.

800 B. Pull-down assays of IntPeri-MBP using PGN sacculi in solutions at different pH (upper gel). The lower
801 gel is a control gel without PGN. S = supernatant, P = pellet.

802 C. Effect of divalent cations and chelators on PGN binding by IntPeri-MBP. Pull-down assays were
803 performed in the presence of either divalent cations or the chelators EDTA or sodium citrate at pH 5.0. S
804 = supernatant, P = pellet.

805 D. Effect of soluble muropeptides on the binding of IntPeri-MBP to PGN sacculi. Pull-down assays were
806 performed with increasing amounts (5-25 µl) of mutanolysin-digested PGN at pH 5.0. S = supernatant, P
807 = pellet.

808 E. Binding of IntPeri-MBP, InvPeri-MBP and MBP to a chitin column. 1 mg of protein was loaded onto a
809 chitin column equilibrated at pH 5.0. The flow through (FT) was collected, the column washed with

running buffer (w) and bound protein was eluted first with a buffer at pH 7.4 followed by elution with 0.3 M NaOH (OH).

F. Binding of IntLysM-MBP, IntHelix1-MBP and IntHelix2-MBP to PGN sacculi. Pull-down assays were performed as in panel A at pH 5.0. S = supernatant, P = pellet.

The results shown are representative of at least two repeated experiments.

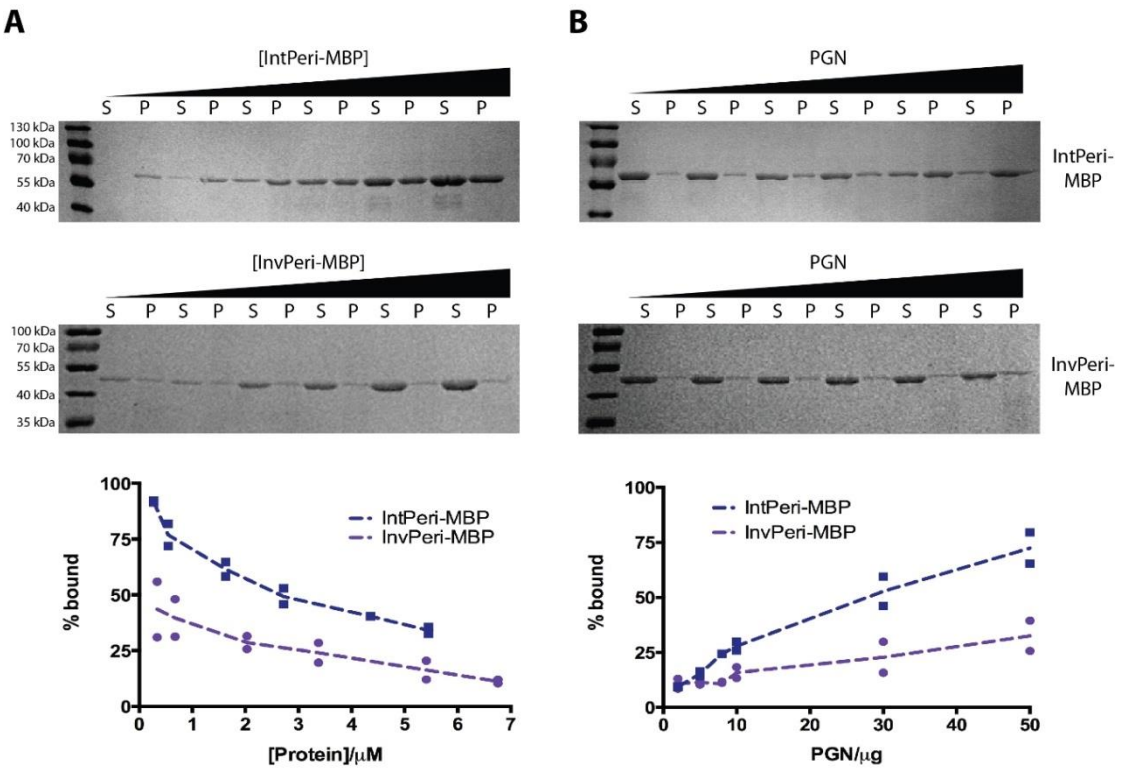


817

818 **Fig. 5**. Quantitative comparison of IntPeri-MBP and InvPeri-MBP binding to PGN.

819 A. Pull-down assays using a concentration series of IntPeri-MBP (upper gel) and InvPeri-MBP (lower gel)
820 against a constant amount of PGN at pH 5.0. The concentrations of IntPeri-MBP and InvPeri-MBP were
821 varied between 0.5 µg and 10 µg per reaction. The graph at the bottom shows relative binding of the
822 proteins to PGN, with the protein concentration expressed as micromoles per litre. Data points from two
823 replicate experiments represent the band intensity of the pellet divided by the sum of the supernatant
824 (S) and pellet (P) intensities for that concentration, multiplied by 100. The curves are plotted based on
825 the average of the two measurements. The bands intensities were quantified using the ImageJ software
826 (Schneider *et al.*, 2012).

827 B. Pull-down assays using a varying amount of PGN sacculi against a constant amount of either IntPeri-
828 MBP (upper gel) or InvPeri-MBP (lower gel). The graph depicts relative binding for each PGN amount (in
829 micrograms). The binding percentage was calculated as for panel A. S = supernatant, P = pellet.

830

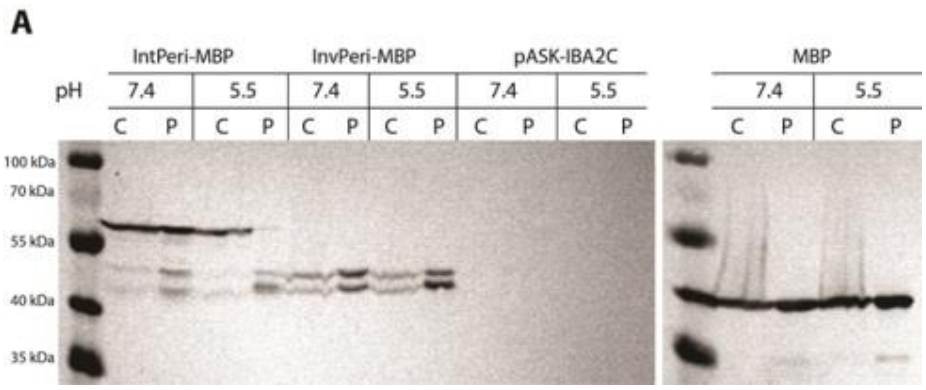


**Fig. 6.** The *Int* periplasmic domain binds to PGN *in vivo*.

*In vivo* binding to peptidoglycan. Cells expressing IntPeri-MBP or InvPeri-MBP periplasmically were grown at pH 7.4 or pH 5.5. The periplasmic fraction was extraction using a modified osmotic shock protocol. Samples from whole cells (C) or the periplasmic fraction (P) were separated by SDS-PAGE and subjected to Western blotting using an anti-MBP antibody. pIBA2C is the vector control, and MBP acts as a control for periplasmic extraction.

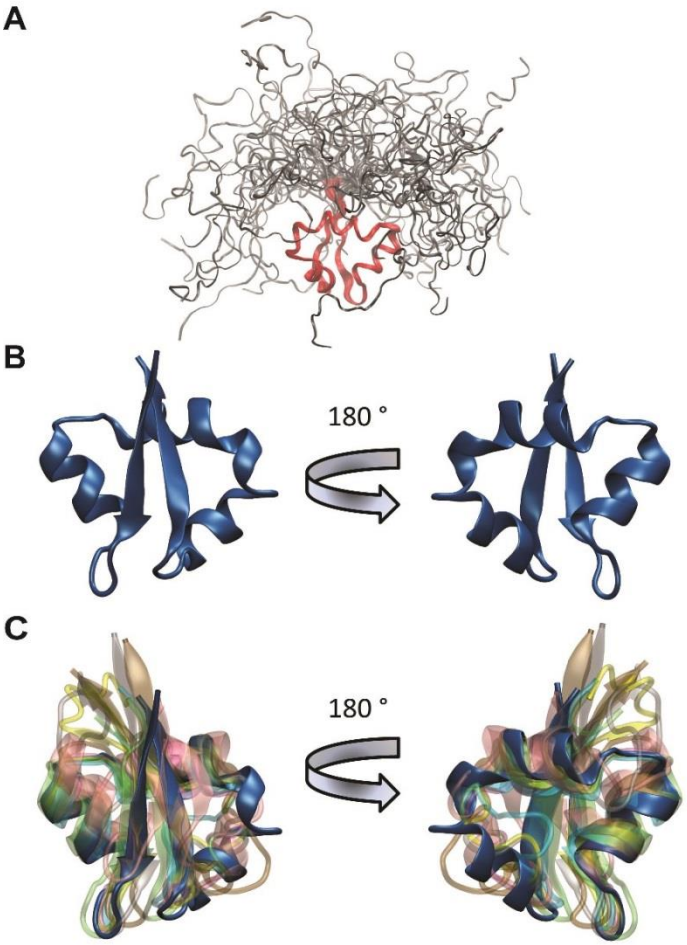


**Fig. 7.** Solution structure of Int LysM

A. Ensemble of 20 acceptable NMR structures for the Int LysM region, showing the LysM itself (highlighted in red) is well defined whereas the N-terminus and C-terminal spacer sequence are disordered.

B. The Int LysM structure in cartoon representation.

C. Superposition of of other LysM structures onto the Int LysM NMR structure (in blue). The structures include bacterial and bacteriophage LysMs (MltD from *E. coli* in green (PDB 1E0G)); YkuD from *B. subtilis* in mauve (1Y7M); gpX from coliphage P2 in salmon (2LTF)), LysMs from fungal protein (LysM1 from Ecp6 of *Cladosporium fulvum* in yellow (4B8V); LysM of CVNH lectin from *Magnaporthe oryzae* in cyan (2L9Y)), a plant protein (LysM1 from AtCERK1 of *A. thaliana* in grey (4EBY)) and a human hypothetical protein (SB145 (2DJP)). The major difference in Int LysM compared to the others is the α-helical region between the C-terminal conserved α-helix and the C-terminal β-strand. The figures were prepared using VMD (Humphrey *et al.*, 1996, http://www.ks.uiuc.edu/Research/vmd/)

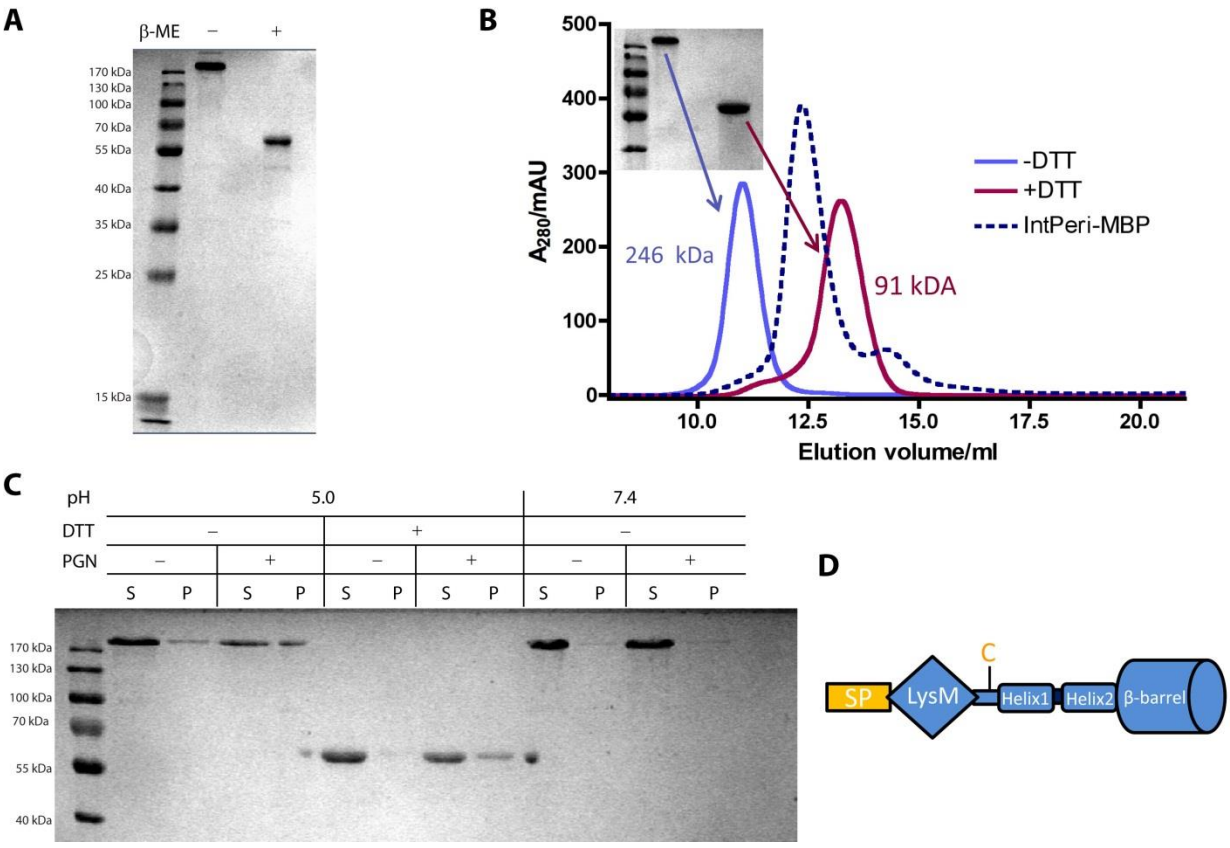


**Fig. 8**. The periplasmic domain of YrInv forms multimers and binds peptidoglycan.

A. Effect of reducing agent on YrInvPeri-MBP. β-ME = β-mercaptoethanol.

B. SEC of YrInvPeri-MBP at pH 7.4 with (magenta) and without DTT(light blue). The inset shows an SDS-PAGE gel of the peaks (no additional reducing agent was added). The expected size for the monomer is 58 kDa. Apparent molecular weights are indicated. The SEC curve for IntPeri-MBP (dashed blue line) is shown for comparison.

C: PGN binding of YrInvPeri-MBP. Pull-downs with or without PGN sacculi was performed at pH 5.0 or pH 7.4. At pH 5.0, pull-down assays were performed either with or without the addition of 10 mM DTT. The small amount of monomeric YrInv seen at the edges of lanes 5 and 10 can be explained by diffusion of the DTT from the neighbouring wells. S = supernatant, P = pellet.

D. Schematic of YrInvPeri periplasmic domain and barrel. The position of the single cysteine in the spacer sequence is indicated.

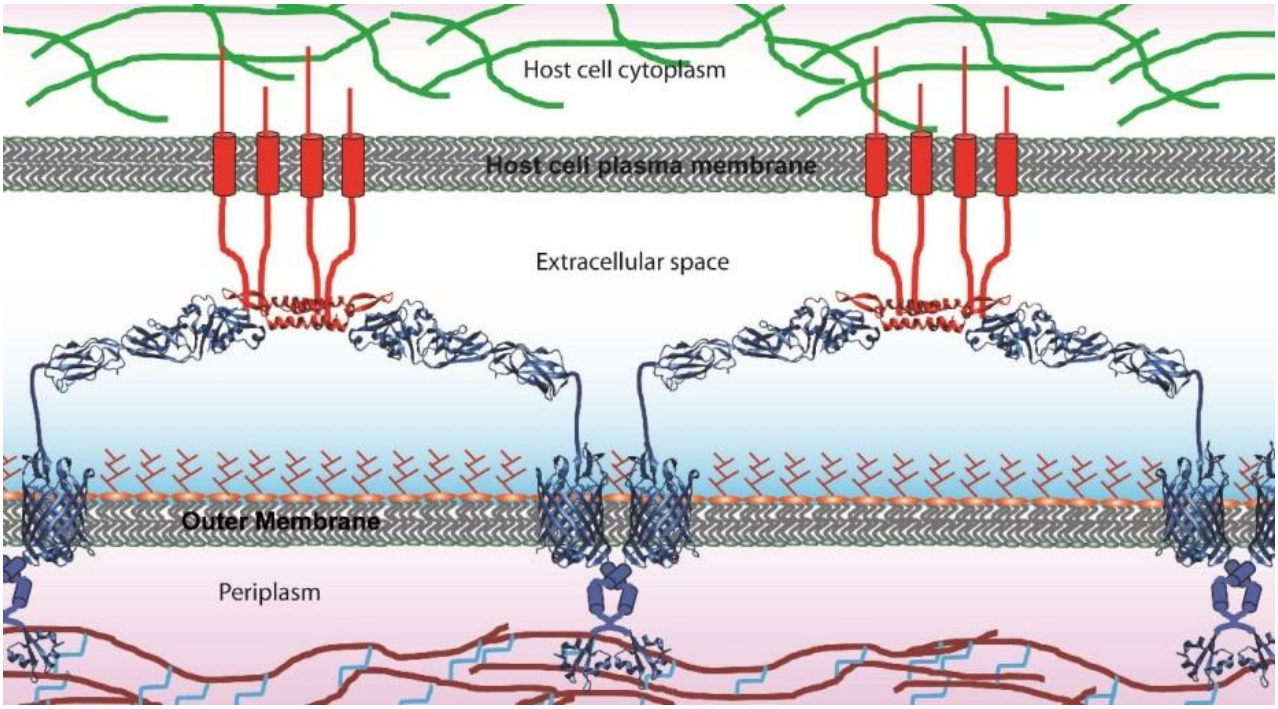


**Fig. 9.** Model for Intimin dimerisation and Tir clustering

Schematic of Int (in blue) bound to Tir (red). Dimerisation of Int through the periplasmic domain in the periplasmic domain leads to a reticular array which promotes Tir clustering and pedestal formation. Dimerisation takes place at two sites within the periplasmic domain: at the C-terminal α-helix and in the spacer sequence between the LysM and the N-terminal α-helix. Where structural information is available, cartoon structures are depicted. Regions of unknown structure are depicted as connecting lines, or cylinders in the case of α-helices. The actin cortex of the host cell is in green, the peptidoglycan backbone in brown and peptide crosslinks in light blue. PDB IDs of the structures used for the figure are 1F02, 4E1S and 2MPW. The structural figures were prepared using VMD (Humphrey *et al.*, 1996, http://www.ks.uiuc.edu/Research/vmd/)